Exploiting Spore-Autonomous Fluorescent Protein Expression to Quantify Meiotic Chromosome Behaviors in *Saccharomyces cerevisiae*

Drew Thacker,*,† Isabel Lam,*,‡ Michael Knop, and Scott Keeney*,†,‡,§,1**

*Molecular Biology Program, Memorial Sloan-Kettering Cancer Center, New York, New York 10065, †Weill Graduate School of Medical Sciences of Cornell University, New York, New York, 10065, ‡Louis V. Gerstner, Jr. Graduate School of Biomedical Sciences, Memorial Sloan-Kettering Cancer Center, New York, New York 10065, §Howard Hughes Medical Institute, New York, New York 10065, and **German Cancer Research Center (DKFZ) and the Center for Molecular Biology of the University of Heidelberg (ZMBH) Alliance, University of Heidelberg, 69120 Heidelberg, Germany

ABSTRACT The budding yeast *Saccharomyces cerevisiae* has proven to be a rich source of information about the mechanisms and regulation of homologous recombination during meiosis. A common technique for studying this process involves microdissecting the four products (ascospores) of a single meiosis and analyzing the configuration of genetic markers in the spores that are viable. Although this type of analysis is powerful, it can be laborious and time-consuming to characterize the large numbers of meioses needed to generate statistically robust data sets. Moreover, the reliance on viable (euploid) spores has the potential to introduce selection bias, especially when analyzing mutants with elevated frequencies of meiotic chromosome missegregation. To overcome these limitations, we developed a versatile, portable set of reporter constructs that drive fluorescent protein expression specifically in only those spores that inherit the reporter. These spore-autonomous fluorescence constructs allow direct visualization of inheritance patterns in intact tetrads, eliminating the need for microdissection and permitting meiotic segregation patterns to be ascertained even in aneuploid spores. As proof of principle, we demonstrate how different arrangements of reporters can be used to quantify crossover frequency, crossover interference, gene conversion, crossover/noncrossover ratios, and chromosome missegregation.

MEIOSIS is a specialized form of cell division in which a single round of DNA replication is followed by two successive rounds of chromosome segregation. In contrast to mitosis, where daughter cells are identical to the mother cell, the progeny of a meiotic cell division have half the genome equivalent of the progenitor cell. This inheritance pattern is achieved by modifying the mitotic chromosome-segregation machinery in three ways (Marston and Amon 2004). First, homologs pair and become physically connected by chiasmata during prophase I, ensuring proper attachment to the meiosis I (MI) spindle. Second, cohesion established between sister chromatids during premeiotic S phase is lost in a stepwise manner: chromatid-arm cohesion is lost during MI, allowing for homologs to segregate to opposite poles, whereas centromeric cohesion is maintained until late meiosis II (MII) to prevent premature separation of sister chromatids (PSSC) and to allow proper attachment to the MII spindle. Third, sister centromeres are oriented toward the same spindle pole in MI, but toward different spindle poles during MII. Failure to follow this series of events can result in abnormal chromosome segregation and formation of aneuploid gametes.

An important challenge is to define the spatial and temporal regulation of these processes, including the control of interhomolog crossing over, which is essential for the establishment of chiasmata. Crossing over is initiated by developmentally programmed DNA double-strand break (DSB) formation catalyzed by the topoisomerase-like protein, Spo11 (Keeney *et al.* 1997). In the budding yeast, *Saccharomyces cerevisiae*, ~160 DSBs are generated per meiosis (Pan *et al.* 2011). On average, ~90 DSBs are repaired as crossovers, and the remainder are repaired as either interhomolog noncrossovers or intersister recombinants (Chen *et al.* 2008; Mancera *et al.* 2008). However, this repair

doi: 10.1534/genetics.111.131326
Manuscript received June 6, 2011; accepted for publication July 25, 2011
Supporting information is available online at http://www.genetics.org/content/suppl/2011/08/12/genetics.111.131326.DC1.
[1]Corresponding author: Howard Hughes Medical Institute, Memorial Sloan-Kettering Cancer Center, 1275 York Ave., Box 97, New York, NY 10065.
E-mail: s-keeney@ski.mskcc.org

process is not random, as each pair of homologous chromosomes requires at least one crossover (often referred to as the obligate crossover) and, when two or more crossovers occur on the same chromosome pair, they tend to be farther apart than expected by chance (referred to as "crossover interference") (Jones 1984; Page and Hawley 2003).

In budding yeast, all four products of a single meiosis can be recovered using a technique called tetrad analysis, which is often used to determine the frequency of crossing over between genetic markers as it provides clear information on the number of reciprocal exchanges in a given interval (Hawley 2007). Tetrad analysis can also identify non-Mendelian segregation events such as gene conversions. However, one drawback to tetrad analysis as currently conducted is the requirement that spores be viable (*i.e.*, able to germinate and form colonies) to score segregation of genetic markers. Moreover, many analyses also require that all four spores of a tetrad are viable.

Elucidating the mechanism and regulation of crossing over and chromosome segregation relies on the study of mutants that alter recombination patterns. For example, mutations in the ZMM family of genes (*ZIP1–4*, *SPO16*, *MSH4/5*, *MER3*) reduce crossing over, elevate homolog nondisjunction, and decrease crossover interference (Börner *et al.* 2004; Chen *et al.* 2008). However, analysis of these mutants is often complicated by low spore viability and temperature-modulated reduction in sporulation efficiency (Börner *et al.* 2004). Furthermore, crossover interference is measured as a probabilistic phenomenon, *i.e.*, one in which observed frequencies of particular recombinant configurations are compared to frequencies predicted under the null hypothesis of a random distribution of crossovers (Berchowitz and Copenhaver 2008). As a result, many individual meioses must be examined to make statistically significant claims regarding the effects of a particular mutation, making data collection a significant limiting factor in studies of crossover control.

To circumvent the dependence on viable spores and to make data collection less time consuming, we sought to develop a series of fluorescent markers that can be scored in spores, independent of germination and colony formation. Developing such markers requires that the promoter controlling fluorescent protein expression remains "off" until after pro-spore membrane formation and cytokinesis. During MII, prospore membrane formation is initiated at the outer plaque (cytoplasmic surface) of the spindle pole bodies (SPB) and expands from these sites of nucleation to engulf the nuclear lobe to which it is anchored via the SPB (Moens 1971; Neiman 2005). Following nuclear division, closure of the prospore membrane occurs via cytokinesis to capture each of the haploid nuclei (Neiman 2005). Spore-wall synthesis is then initiated in the lumen between the two prospore membrane-derived membranes followed by the collapse of the anucleate mother cell to form the ascus (Lynn and Magee 1970; Neiman 2005).

Here, we show that spore-autonomous fluorescent markers allow crossing over, crossover interference, gene conversion, and chromosome missegregation to be detected and quantified directly in budding-yeast tetrads. Fluorescent marker segregation can be scored even in inviable aneuploid spores, facilitating analysis of mutants with elevated chromosome missegregation. By eliminating tetrad microdissection, large data sets can be generated rapidly for mutant strains under various culture conditions.

Materials and Methods

Yeast strains and plasmids

Strains were of the SK1 background (Supporting Information, Table S1). The m-Cerulean (CFP), tdTomato (RFP), and GFP* markers (Table 1) were engineered using PCR. For m-Cerulean, 596 bp of *YKL050c* promoter DNA (upstream of the start codon) was amplified from *S. bayanus* genomic DNA and fused to the 5′ end of the m-Cerulean open reading frame (plasmid from Jeffrey Smith, Memorial Sloan-Kettering Cancer Center). The *PGK1* terminator was then amplified from *S. bayanus* (416 bp downstream of the *PGK1* stop codon), fused to the 3′ end of m-Cerulean, and cloned into pCR2.1. *Eco*RI sites (added to the 5′ *YKL050c* primer and 3′ *PGK1* terminator primer) were used to excise the fragment from pCR2.1 and subclone it into pRS404 (Sikorski and Hieter 1989). Targeting this plasmid to *THR1* was achieved by PCR-amplifying Saccharomyces Genome Database (SGD) coordinates 160333–160951 on chromosome VIII (5′ and 3′ primers contain *Sac*II restriction sites), digesting the PCR product with *Sac*II, and cloning the fragment into pRS404-m-Cerulean. To linearize the plasmid for transformation, an *Afl*II restriction site was introduced into the *THR1*-targeting region by Quikchange Site-directed Mutagenesis (Stratagene) with the primers 5′-CATTAACAATACAGATAATGAATCTTAAGTTGTTTTCAGTCTC and 5′-GAGACTGAAAACAACTTAAGATTCATTATCTGTATTGTTAATG.

For tdTomato, 607 bp of *YKL050c* promoter DNA and 412 bp of *PGK1* terminator DNA from *S. kudriavzevii* was fused to the tdTomato open reading frame (plasmid from Mark Lundquist, Weill Cornell) and cloned into pCR2.1. *Bam*HI was used to excise the fragment from pCR2.1 and subclone it into pRS305 (Sikorski and Hieter 1989). A silent

Table 1 Plasmids

Plasmid number	Description
pSK691	$P^{YKL050c}$-*RFP* in pRS305 (*LEU2*)
pSK692	$P^{YKL050c}$-*CFP* in pRS404 (*TRP1*)
pSK693	$P^{YKL050c}$-*RFP* in pRS305 (*LEU2*), targets integration to *CEN8*
pSK694	$P^{YKL050c}$-*CFP* in pRS404 (*TRP1*), targets to *CEN8*
pSK695	$P^{YKL050c}$-*CFP* in pRS404, targets to *THR1*
pSK724	P^{GPD1}-*gfp*-atg* (*Bam*HI–*Sal*I fragment) in pMJ349 (*URA3*) targets to *ARG4*
pSK725	P^{GPD1}-*gfp*-R215X* (*Bam*HI–*Sal*I fragment) in pMJ349 targets to *ARG4*
pSK726	$P^{YKL050c}$-*GFP** in pRS306 (*URA3*)
pSK729	$P^{YKL050c}$-*GFP** in pRS306 (*URA3*) targets to *ARG4*

mutation was introduced into the *LEU2* coding sequence on the plasmid using site-directed mutagenesis to destroy the *Afl*II restriction site. Targeting this construct and the m-Cerulean construct to *CEN8* was achieved by PCR-amplifying SGD coordinates 105705–106240 on chromosome VIII (5′ and 3′ primers contain *Sac*II restriction sites), digesting the PCR product with *Sac*II, and cloning the fragment into pRS305-tdTomato or pRS404-m-Cerulean. To linearize the plasmids for transformation, an *Afl*II restriction site was introduced into the *CEN8*-targeting region by site-directed mutagenesis with the primers 5′-CTGAAACCGTCAACTTAAGAAGGGATG TGATATATTCAAAATGG and 5′-CCATTTTGAATATATCACAT CCCTTCTTAAGTTGACGGTTTCAG.

For GFP*, 603 bp of *YKL050c* promoter DNA and 416 bp of *PGK1* terminator DNA from *S. mikatae* was fused to the Green Lantern open reading frame cloned into pCR2.1. *Eco*RI was used to excise the fragment from pCR2.1 and subclone it into pRS306. The Green Lantern emission spectrum significantly overlapped with the cyan epifluorescence channel on our microscope, causing ambiguity in scoring Gfp^+ and Cfp^+ spores (data not shown). To circumvent this issue, the green emission spectrum was shifted to yellow by introducing five mutations in Green Lantern (T65G, V68L, Q69M, S72A, and T203Y) (Griesbeck *et al.* 2001) using site-directed mutagenesis. We refer to this modified protein as "GFP*" hereafter. Targeting to *ARG4* was achieved by PCR-amplifying SGD coordinates 140928–142149 on chromosome VIII (5′ and 3′ primers contain *Sac*II restriction sites), digesting the PCR product with *Sac*II, and cloning the fragment into pRS306-Green*. *Afl*II was used to linearize the plasmid for transformation.

For the *gfp** heteroalleles, the *Taq*I fragment (653 bp) of the *GPD1* promoter (the 5′ primer has a *Bam*HI site) and a 908-bp fragment (containing 765 bp of the *PGK1* terminator) starting at the *Pst*I site and extending in the 3′ direction (the 3′ primer has a *Sal*I site) were amplified from plasmid pG1 (Schneider and Guarente 1991) and fused to the Green Lantern open reading frame. The resulting fragment was cloned into pCR2.1. We used site-directed mutagenesis to destroy a *Bam*HI restriction site in the Green Lantern open reading frame and *Sal*I and *Eco*RI sites in the PGK terminator sequence. A *Bam*HI–*Sal*I double digest excised the fragment from pCR2.1 for subcloning into pMJ349, replacing the *arg4-bgl* allele (Borde *et al.* 1999). The green emission spectrum was shifted to yellow as described above. Site-directed mutagenesis was used to change the start codon (ATG) in one *GFP** allele to ACG (*gfp*-atg*) and introduce a premature stop (TGA) at codon 215 in the other (*gfp*-R215X*). *Eco*RI sites were reintroduced into the resulting plasmid by Quickchange Multi Site-directed Mutagenesis (Stratagene) with the primers 5′-GCCCTTTCGTCTTCAAG AATTCATCTGTAAACTACAACCACC and 5′-GACAAAATGCC ATGAGAATTCCCTCATGTTTGACAGCTTATCATCG. Targeting this construct to *ARG4* was achieved by PCR-amplifying SGD coordinates 140917–142168 on chromosome VIII (5′ and 3′ primers contain *Eco*RI restriction sites), digesting the PCR product with *Eco*RI and cloning the fragment into pMJ349-Green*. *Afl*II was used to linearize the plasmids for transformation.

The *gfp** heteroalleles were flanked by previously described *Nde*I restriction site polymorphisms (Martini *et al.* 2006), introduced by two-step gene replacement, and confirmed by Southern blotting of genomic DNA. The *MSH5* deletion was made by replacing the coding sequence with the *kanMX4* cassette (Wach *et al.* 1994).

DSB measurements and random spore analysis

Cultures of *sae2*Δ strains were grown in liquid YPA (1% yeast extract, 2% Bacto peptone, 1% potassium acetate) for 13.5 hr at 30°, harvested, resuspended in 2% potassium acetate, and incubated at 30°. Samples were collected at 0 and 8 hr, and DNA was prepared for conventional agarose electrophoresis (Murakami *et al.* 2009). DNA was digested with *Bgl*II and probed with part of the *YHR018c* open reading frame (SGD coordinates 140353–140717). Blots were quantified by PhosphorImager. DSBs are expressed as the percentage of total radioactivity in the lane after background subtraction, not including material in wells. Random spore analysis was performed as previously described (Martini *et al.* 2006). Map distances (cM ± SE) were calculated using the Stahl Lab Online Tools (http://www.molbio.uoregon.edu/~fstahl/).

Meiotic time courses and analysis of events by microscopy and FACS

For experiments performed at 23° and 30°, the sporulation protocol was as described above, with sporulation medium pre-equilibrated to the appropriate temperature. For experiments performed at 33°, cells were sporulated at 30° for 2 hr and then shifted to 33°. All cultures were sporulated for 48–60 hr. Tetrads were briefly sonicated and then analyzed using a Zeiss Axiovert 200 microscope. Diploid cells heterozygous for each fluorescent marker were sporulated, harvested, treated with 500 μg zymolyase (20T), diluted in 0.1% Tween-20, sonicated, and then analyzed using a Cytomation MoFlo Cell Sorter. To enrich for Gfp^{*+} tetrads in the crossover/noncrossover analysis, cells were harvested and resuspended in an equal volume of 0.1% Tween-20, sonicated briefly, and then sorted.

Incidental crossover analysis using NdeI restriction site polymorphisms

Individual Gfp^{*+} spores were isolated by FACS and plated onto rich medium. The resulting colonies were replica-plated onto media lacking tryptophan or leucine to identify cells containing the *CFP*::*TRP1* marker or the *RFP*::*LEU2* marker, respectively. DNA was extracted from spores with both parental and nonparental configurations of these markers and analyzed to determine the configuration of the flanking *Nde*I polymorphisms by PCR amplification followed by digestion with *Nde*I (Martini *et al.* 2006).

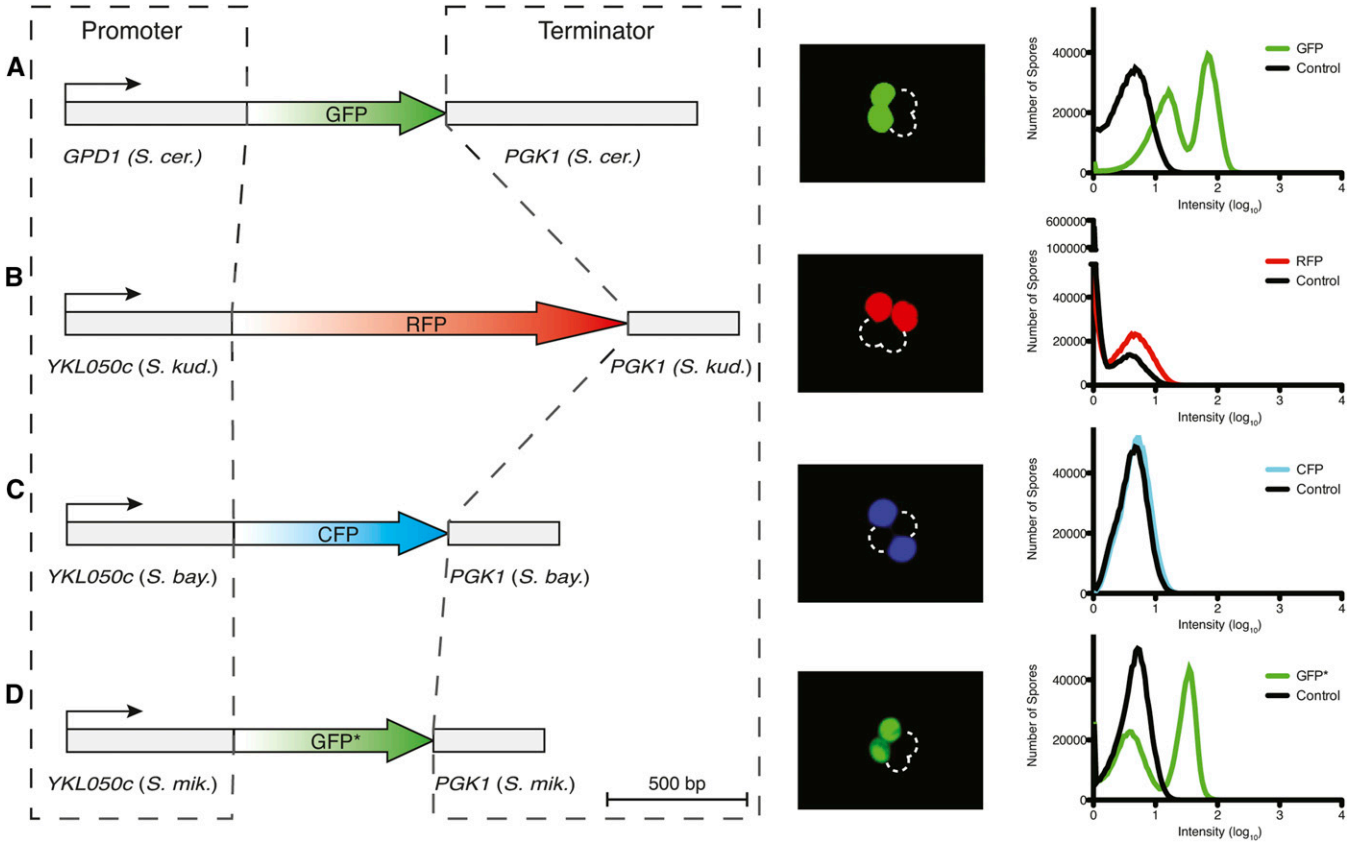

Figure 1 Promoter and terminator combinations to drive spore-autonomous expression of fluorescent proteins. Constructs are diagrammed to scale on the left of A–D, with promoters and terminators cloned from the indicated species. Epifluorescent images of whole tetrads and FACS profiles of individual spores are shown, derived from diploid cells hemizygous for the corresponding construct. Spores from a diploid strain lacking fluorescent markers were used as a control.

Results

Versatile, portable constructs that drive spore-autonomous fluorescent protein expression

An elegant fluorescent method was developed for visual analysis of recombination events in tetrads of *Arabidopsis thaliana* pollen grains, facilitating measurement of genetic distances and crossover interference (Francis *et al.* 2007). We wanted to develop a similar assay for *S. cerevisiae*, in which fluorescent protein expression could be detected only in spores that inherit a copy of the reporter gene, termed "spore-autonomous" expression.

We examined P^{GPD1} and $P^{YKL050c}$, two promoters previously reported to give this expression pattern (Gordon *et al.* 2006; Mell *et al.* 2008). When individual spores from a P^{GPD1}-*GFP* hemizygote were analyzed by FACS, equally abundant GFP-high and GFP-low populations were observed, with an approximately fourfold average difference in GFP intensity between them (Figure 1A). Notably, spores that did not inherit P^{GPD1}-*GFP* (the GFP-low population) also had GFP levels above background (Figure 1A), likely due to vegetative expression.

$P^{YKL050c}$ exhibited less background fluorescence, enabling ready detection by microscopy of spore-autonomous expression in strains hemizygous for $P^{YKL050c}$-*RFP* or $P^{YKL050c}$-*CFP* (Figures 1, B and C). However, these signals could not be detected using any of several cytometers evaluated (Figure 1, B and C, and data not shown). In contrast, spore-autonomous expression was readily detected by both microscopy and FACS for a modified version of GFP ($P^{YKL050c}$-*GFP**), which was engineered to reduce emission in the cyan epifluorescence channel (Figure 1D; see *Materials and Methods*). $P^{YKL050c}$-*GFP** gave approximate ninefold difference in fluorescence intensity between the negative and positive spore populations (Figure 1D).

To minimize the possibility of recombination between reporters, we isolated *YKL050c* promoter and *PGK1* terminator sequences from different *Saccharomyces* species: *S. mikatae*, *S. kudriavzevii*, and *S. bayanus* (Figure 1). The percentage identity between the sequences is <65.8% and <82.9% for the promoters and terminators, respectively (Table S2). The fluorescent protein-coding sequences also have low sequence identity (<81.0%, excluding the Green Lantern and GFP* comparison) (Table S2). Each reporter cassette has a different selectable marker (*RFP*::*LEU2*, *CFP*::*TRP1*, *GFP**::*URA3*) on integration vectors that provide portability by allowing targeting throughout the genome. Below, we show proof-of-principle experiments for a series

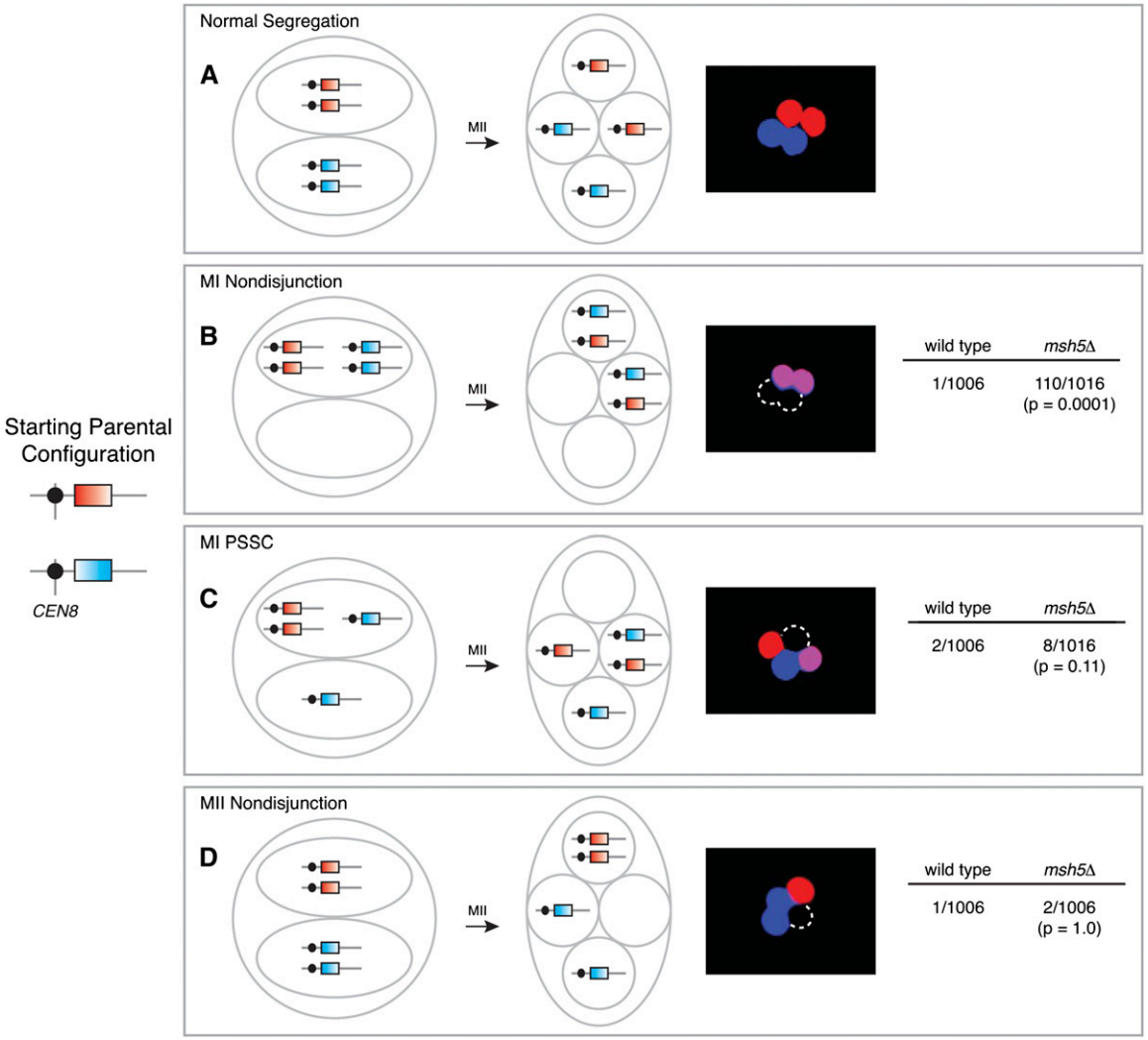

Figure 2 Chromosome missegregation assay. $P^{YKL050c}$-*RFP* and $P^{YKL050c}$-*CFP* were integrated in allelic positions near *CEN8*. Cartoons show configuration of the markers after MI and MII for normal segregation and different types of missegregation, and micrographs show examples of each segregation pattern. Data on the right of B–D show the frequency of each type of missegregation in diploid wild-type and *msh5*Δ strains, pooled from two independent cultures of each strain (≥501 tetrads/culture). Statistical significance was evaluated by Fisher's exact test (two-tailed *P*-value). The complementary arrangement for MII nondisjunction was also observed (one Cfp$^+$ spore, two Rfp$^+$ spores, and one nonfluorescent spore; data not shown).

of configurations to score different meiotic chromosome behaviors.

Chromosome segregation

By integrating $P^{YKL050c}$-*RFP* and $P^{YKL050c}$-*CFP* at allelic positions near the centromere of chromosome VIII, we can score MI nondisjunction, MI PSSC, and MII nondisjunction. Proper chromosome segregation yields tetrads with two Rfp$^+$ spores and two Cfp$^+$ spores (Figure 2A). However, if homologs fail to disjoin at MI, two spores will be both Rfp$^+$ and Cfp$^+$ and two will be nonfluorescent (Figure 2B), whereas PSSC during MI yields tetrads containing one Rfp$^+$ and Cfp$^+$ spore, one Rfp$^+$ spore, one Cfp$^+$ spore, and one nonfluorescent spore (Figure 2C). Both types of missegregation give unambiguous fluorescent patterns because all four marked chromatids (two red and two cyan) can be directly observed.

In the event of MII nondisjunction, two spores inherit only the cyan (or red) marker, one spore inherits both of the red (or cyan) markers, and one spore is nonfluorescent (Figure 2D). This pattern is potentially ambiguous because a nonfluorescent spore could also arise through failure to activate the *YKL050c* promoter. For example, if spores are damaged or if there are spore-autonomous *trans*-acting loci essential for expression from $P^{YKL050c}$ and the chromosome(s) carrying such loci does not segregate with the chromosome carrying the fluorescent markers, then a spore will be nonfluorescent. Such false negatives would potentially be more frequent in mutants with elevated missegregation rates. To determine the proportion of tetrads with damaged spores, we constructed a diploid strain homozygous for $P^{YKL050c}$-*RFP* integrated near the centromere of chromosome VIII and for P^{GPD1}-*GFP* integrated at *LEU2* on chromosome III. Events where both chromosome III and chromosome VIII do not

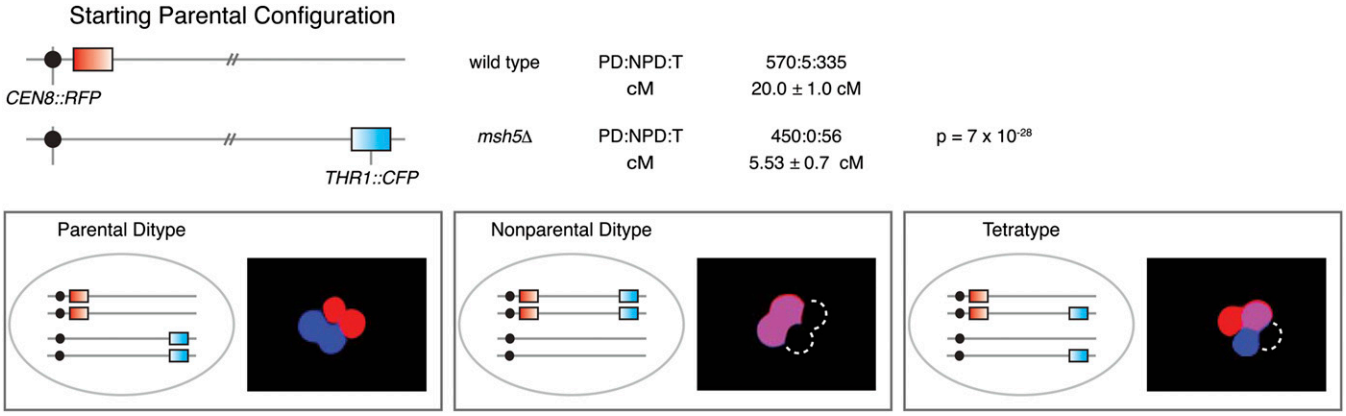

Figure 3 Two-factor cross to measure genetic distance. $P^{YKL050c}$-*RFP* and $P^{YKL050c}$-*CFP* were integrated at *CEN8* and *THR1*, respectively, and segregation of these markers was assessed in wild-type and *msh5*Δ strains (one culture of each). Cartoons show possible configurations of markers, and micrographs show examples of corresponding tetrads. The frequency of parental ditype (PD), nonparental ditype (NPD), and tetratype (T) tetrads is shown, along with calculated map distances (±SE). For the *msh5*Δ strain, NPDs were scored as MI nondisjunction events (see *Chromosome segregation*) and thus not included in the map distance calculations. Statistical significance was evaluated by *G* test for the distribution of tetrad classes for each strain.

disjoin at MII and segregate to the same spindle pole should be exceedingly rare; therefore, any spore that is completely nonfluorescent is likely damaged or dead. Of 2147 tetrads analyzed, we did not observe a single nonfluorescent spore (<0.05%). The frequencies of chromosome III (24/2147) and chromosome VIII (9/2147) MII nondisjunction observed in the same experiment were significantly greater than the frequency of nonfluorescent spores ($P = 0.0001$ and $P = 0.004$, respectively).

As validation of this assay, we analyzed wild-type and *msh5*Δ cells. Msh5 is a meiosis-specific MutS homolog that does not exhibit mismatch repair activity (Hollingsworth *et al.* 1995) and that stabilizes intermediates in the crossover repair pathway (Börner *et al.* 2004; Snowden *et al.* 2004). Deleting *MSH5* increases MI nondisjunction, but rates of MI PSSC and MII nondisjunction are relatively unaffected (Sym and Roeder 1994; Hollingsworth *et al.* 1995). As expected, all forms of chromosome missegregation were rare in wild type, whereas the *msh5*Δ mutant showed 109-fold elevation of MI nondisjunction without a change in PSSC or MII nondisjunction (Figure 2, B–D). The MI nondisjunction frequency (10.8%) was lower than reported for chromosome III (15%) (Hollingsworth *et al.* 1995), presumably because chromosome III, being shorter, is more likely to fail to generate a crossover (Mancera *et al.* 2008).

Measuring crossover frequency and interference

In budding yeast, the most common way to quantify crossing over involves dissecting tetrads and scoring spore-derived colonies for segregation of heterozygous markers by replica-plating to selective media or by physical analysis of DNA sequence polymorphisms. This approach often requires that all four spores of a tetrad be viable, especially for analysis of crossover interference. It can take more than a week to perform dissections and score phenotypes for 1000 meioses for a wild-type strain sporulated under a single condition, and even longer for mutants that yield fewer four-spore viable tetrads.

Our fluorescent constructs eliminate tetrad dissection and largely alleviate spore viability requirements, thus significantly reducing the time to perform a genetic analysis. As proof of principle, we integrated $P^{YKL050c}$-*CFP* at the *THR1* locus on chromosome VIII and mated this strain with one that has $P^{YKL050c}$-*RFP* integrated near *CEN8* (Figure 3). In wild type, we observed a genetic distance of 20.0 cM (Figure 3), comparable to that previously reported for the same chromosomal region but scored with different genetic markers (20.1 cM) (Martini *et al.* 2006). In a *msh5*Δ mutant, the crossover frequency was reduced 3.6-fold (Figure 3), within the expected range of 2- to 5-fold (Malkova *et al.* 2004; Nishant *et al.* 2010).

By also integrating $P^{YKL050c}$-*GFP** at *ARG4* (Figure 4, A–C), we set up a three-factor cross that allows crossover interference to be examined using the method of Malkova *et al.* (2004). Briefly, tetrads are divided into two classes: those that have a detectable crossover in a reference interval [tetratypes (T) and nonparental ditypes (NPD)] and those that do not [parental ditypes (PD)]. For each class, we assessed the crossover frequency in the adjacent test interval. If crossing over in the reference interval is associated with a significantly lower crossover frequency in the test interval, then positive crossover interference is present between the two intervals. For example, a wild-type strain sporulated at 30° exhibited a crossover frequency of 5.90 cM in the test interval *ARG4-THR1* when there was no crossover in the reference interval *CEN8-ARG4*, but only 1.37 cM when the reference interval did display a crossover (Table S3). Taking the ratio of the two values (1.37/5.90 = 0.23) gives an estimate of the strength of interference—the lower the value, the stronger the interference.

Interference was observed between the *CEN8-ARG4* and *ARG4-THR1* intervals at 30° in wild type but not in a *msh5*Δ mutant (Figure 4E and Table S3), similar to previous results

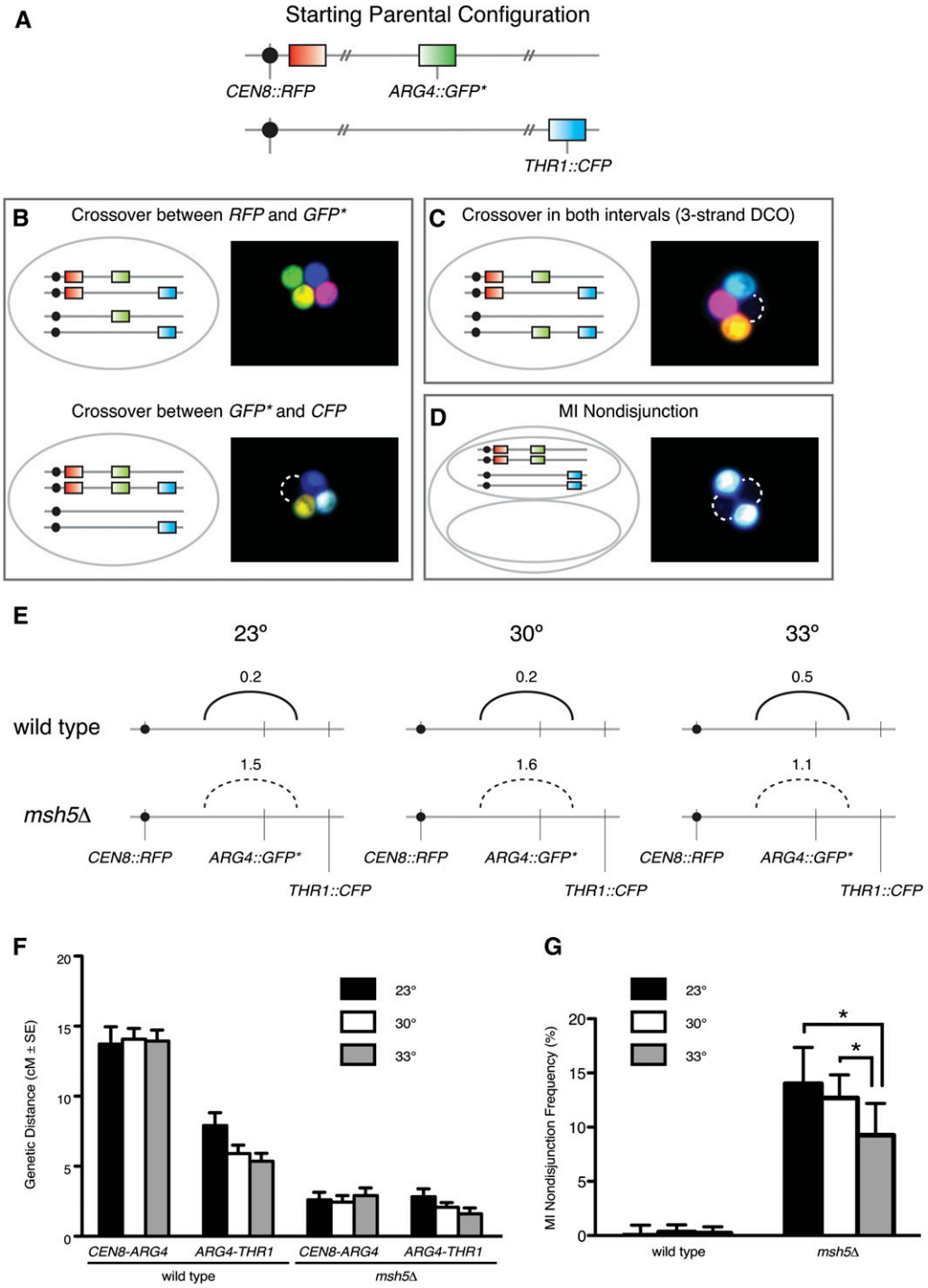

Figure 4 Using a three-factor cross to measure crossover interference. (A) The configuration of $P^{YKL050C}$-*RFP*, $P^{YKL050C}$-*GFP**, and $P^{YKL050C}$-*CFP*. (B) Schematic representations and micrographs illustrating the configuration of markers when there is a recombination event in either the *CEN8-ARG4* interval or the *ARG4-THR1* interval. (C) A tetrad with a recombination event in both the *CEN8-ARG4* and *ARG4-THR1* intervals. This is a three-strand double crossover (DCO) between *CEN8* and *THR1*. Two-strand and four-strand DCOs (one crossover in each interval) can also be identified but are not shown here. (D) An MI nondisjunction tetrad. This segregation pattern is ambiguous because it can also arise from a four-strand DCO in the *ARG4-THR1* interval (see *Measuring crossover frequency and interference*). A four-strand DCO in the *CEN8-ARG4* interval is unambiguous (not shown). (E) Interference was assessed at 23°, 30°, and 33°. Numbers above the arcs are the average interference ratios for the interval pair. The smaller the ratio, the greater the apparent strength of interference. Solid arcs indicate significant interference; dashed arcs indicate that there was no statistically significant evidence for interference. The statistical significance was evaluated by *G* test for the distribution of tetrad classes in the test interval with *vs.* without a crossover in the adjacent interval. (F) Genetic distances for wild-type and *msh5*Δ strains sporulated at the indicated temperatures. (G) MI nondisjunction. Error bars are the 95% confidence interval of the proportion. An asterisk denotes a statistically significant difference (Fisher's exact test (two tailed *P*-value); $P < 0.05$).

for this region (Martini *et al.* 2006 and Neil Hunter, personal communication). A major advantage of the fluorescence-based assay is the ability to look easily at multiple conditions once strains are constructed, for example, altering temperature and/or sporulation medium, adding chemicals that affect key cellular processes, etc. To illustrate the ease with which alternative analyses can be conducted, we also measured crossing over in wild-type and *msh5*Δ strains at 23° and 33°. In both strains, varying temperatures across this range did not significantly alter either crossover frequencies (Figure 4F and Table S3) or presence or absence of interference (Figure 4E and Table S3).

In this three-factor cross, MI nondisjunction and a four-chromatid double crossover (i.e., NPD) in the *ARG4-THR1* interval will give the same fluorescence pattern, with two spores each inheriting all three markers and two spores inheriting none (Figure 4D). However, <0.07% of tetrads displayed an NPD in the *CEN8-ARG4* interval, which can be scored unambiguously (3 of 4397 total tetrads for wild type and *msh5*Δ mutant combined; Table S3). Double crossovers

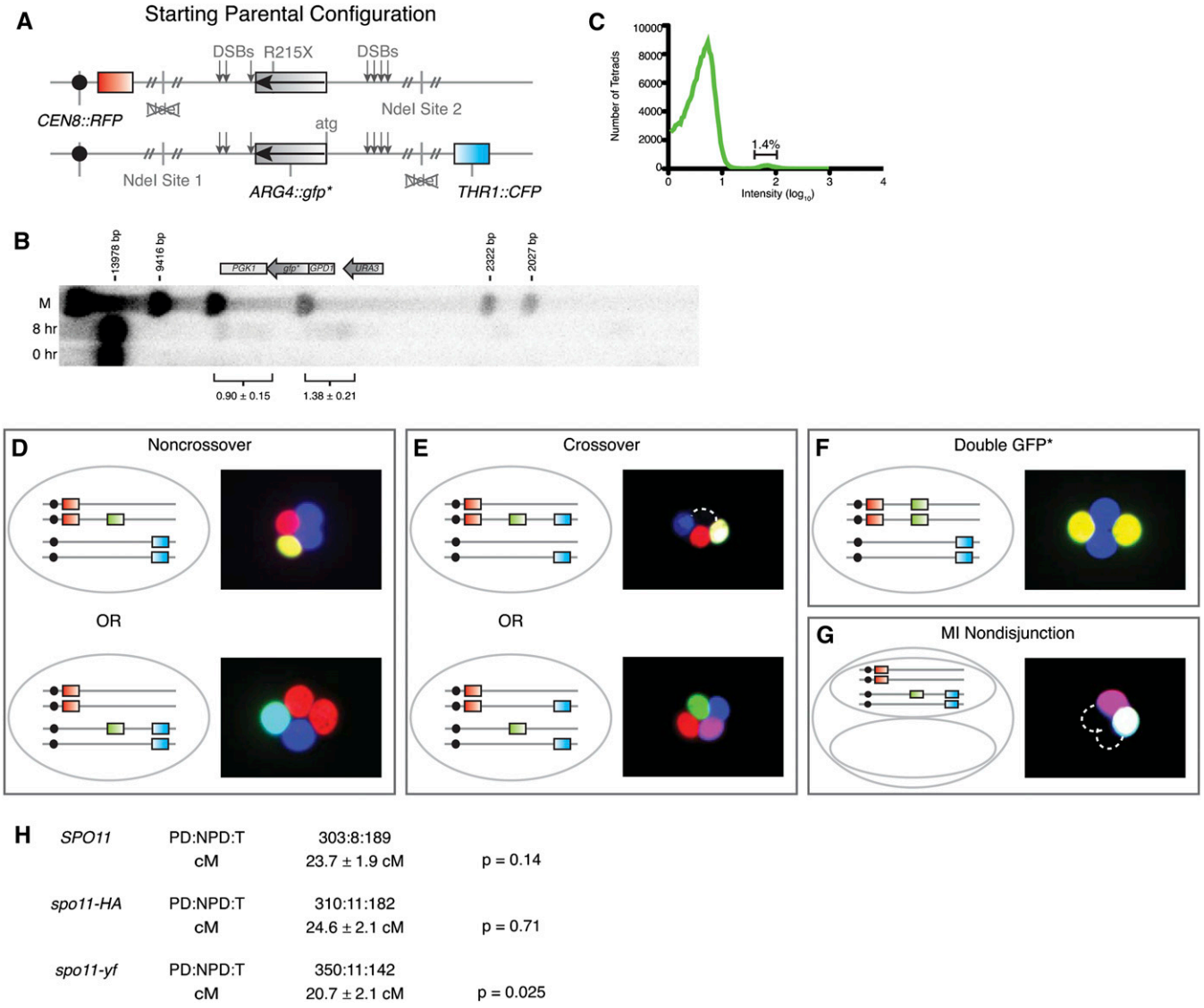

H				
	SPO11	PD:NPD:T	303:8:189	
		cM	23.7 ± 1.9 cM	p = 0.14
	spo11-HA	PD:NPD:T	310:11:182	
		cM	24.6 ± 2.1 cM	p = 0.71
	spo11-yf	PD:NPD:T	350:11:142	
		cM	20.7 ± 2.1 cM	p = 0.025

Figure 5 Fluorescent crossover/noncrossover assay. (A) The configuration of P^{GPD1}-*gfp** heteroalleles, *Nde*I restriction site polymorphisms, and flanking $P^{YKL050c}$-*RFP* and $P^{YKL050c}$-*CFP* markers is diagrammed. The relative frequency and position of DSBs are indicated with arrows. (B) DSBs at the *ARG4*::*gfp** insertion site. A Southern blot of *Bgl*II-digested genomic DNA from a meiotic culture of a strain homozygous for *sae2*Δ and containing the fluorescence recombination reporter diagrammed in A. (C) FACS analysis of Gfp*$^{+}$ recombinant tetrads. Approximately 1.6×10^5 tetrads were analyzed. (D and E) Schematic and micrographs illustrating the configuration of markers when there is a noncrossover gene conversion (D) or either a gene conversion with an associated crossover or a crossover between the two *gfp** mutations (E). (F) Tetrad with two Gfp*$^{+}$ spores, possibly generated from premeiotic recombination or complex meiotic events. (G) MI nondisjunction, or (expected to be very rare) one class of four-strand double crossover. (H) Map distances (±SE) were calculated for the *RFP–CFP* interval in strains carrying the construct diagrammed in A. Statistical significance was evaluated by *G* test for the distribution of tetrad classes for each strain; *spo11-HA* and *spo11-yf* were compared to *SPO11*, whereas the *SPO11* strain here was compared to *SPO11* in Figure 3.

are expected to be even rarer in the smaller *ARG4-THR1* interval and thus are substantially less frequent than MI nondisjunction, especially in the *msh5*Δ mutant (Figure 2). We therefore counted all tetrads with the fluorescence pattern shown in Figure 4D as MI nondisjunction events.

At all temperatures tested, the wild-type strain exhibited a low frequency of MI nondisjunction (≤0.3%) (Figure 4G and Table S3). In the *msh5*Δ mutant, MI nondisjunction at 30° (12.7%) (Figure 4G and Table S3) was similar to that observed with the chromosome missegregation assay (Figure 2B), and comparable frequencies were observed at 23° (Figure 4G and Table S3). In contrast, at 33°, a significantly lower frequency was observed (9.2%) (Figure 4G and Table S3), in agreement with published data showing temperature-modulated chromosome III segregation patterns in *msh5* mutants without corresponding changes in crossover frequency (Chan *et al.* 2009).

It is noteworthy that, once the sporulated cultures were in hand, it took <2 hr to score segregation patterns in 500–1000 tetrads for each of two strains at three temperatures;

conventional tetrad dissection and replica-plating likely would have taken many weeks. We conclude that spore-autonomous fluorescent constructs allow much quicker and easier analysis of crossover frequency and interference compared to classical methods. Moreover, MI nondisjunction can be scored concurrently, further reducing the time for comprehensive analysis of a given mutant.

Quantifying crossovers and noncrossovers at a single locus

Heteroallele recombination reporter: Figure S1 diagrams one way to compare relative frequencies of crossovers and noncrossovers at a single locus (Martini *et al.* 2006). Strains heterozygous for different *arg4* mutant alleles are sporulated and then Arg$^+$ recombinants are selected from random spore populations, and the configuration of flanking markers is determined by replica-plating onto selective media. This is a sensitive assay because the Arg$^+$ selection step allows large numbers of recombinant chromosomes to be scored, but a drawback is that the random spore analysis squanders a strength of yeast, namely, the ability to recover all four products of a single meiosis. Moreover, viable spores are required, which can create a sampling bias that affects observed crossover/noncrossover ratios because crossovers (but not noncrossovers) promote viability by ensuring proper chromosome segregation.

To address these limitations, we designed a fluorescence-based assay to measure crossovers and noncrossovers in tetrads in a manner less dependent on spore viability. We used *GFP** as the central recombination reporter, introducing a single point mutation that destroys the start codon in one allele and a single point mutation that creates a premature stop at codon 215 in the other allele (Figure 5A). Spores that inherit either allele do not fluoresce, but functional *GFP** can be generated by recombination. Since premeiotic (non-spore-autonomous) expression of mutant *gfp** does not yield functional fluorescent protein, we used the *S. cerevisiae GPD1* promoter. The P^{GPD1}*-gfp** alleles were integrated at *ARG4* within the context of plasmid sequences that provide DSB hotspots (Wu and Lichten 1995; Borde *et al.* 1999). DSBs form predominantly at two locations within the integrated plasmid-associated DNA: upstream of the *GPD1* promoter and near the 3′ end of *gfp** extending into the *PGK1* terminator (Figure 5B). Although DSBs form with a higher frequency near the *GPD1* promoter (1.38 ± 0.21%), the majority of these DSBs occur ~900–1100 bp from the *gfp*-atg* mutation (Figure 5B). DSB formation in the *PGK1* terminator occurs at a lower frequency (0.90 ± 0.15%); however, a portion of these DSBs are generated near the 3′ end of *gfp**, only ~50–200 bp from the *gfp*-R215X* mutation (Figure 5B). Different spore-autonomous markers were integrated in flanking positions to enable scoring of crossovers and noncrossovers (Figure 5A).

From a strain heterozygous for the P^{GPD1}*-gfp** alleles, ~1.4% of tetrads contained a Gfp*$^+$ spore(s) (Figure 5C). We sorted Gfp*$^+$ tetrads to enrich for recombinants and then scored the flanking marker configurations by microscopy (Figure 5, D and E). In 61.5% of Gfp*$^+$ tetrads from a wild-type strain, the Gfp*$^+$ spore had a nonparental (crossover) configuration of flanking markers (Table 2A and Figure 5E).

We also analyzed a *msh5Δ* strain. By FACS, fewer Gfp*$^+$ counts were observed on a per-cell basis (0.22%). This lower apparent recombination frequency is at least partly due to reduced sporulation efficiency (56% for *msh5Δ vs.* >90% for wild type at 30°). Cells that fail to form spores inflate the apparently nonrecombinant population when scored by FACS. Nonetheless, it was possible to rapidly score crossover and noncrossover outcomes in this mutant. Among sorted tetrads with a Gfp*$^+$ spore, that spore had a crossover configuration of flanking markers 41.7% of the time (Table 2A), which is significantly decreased relative to wild type but similar to results using the *arg4* heteroallele assay (Table 2B). This result is as expected from the reduced crossover frequency in the *msh5Δ* mutant.

Crossover homeostasis: Cells that experience lower numbers of DSBs compensate by having a higher percentage of breaks that become crossovers (Martini *et al.* 2006; Chen *et al.* 2008; Roig and Keeney 2008). This phenomenon, known as crossover homeostasis, can be assayed using *arg4* heteroalleles in a series of *spo11* hypomorphic mutants with reduced DSB formation: the fraction of Arg$^+$ recombinants that have a crossover configuration increases as Spo11 activity decreases (Martini *et al.* 2006) (Table 2B). To evaluate utility of the *gfp** heteroalleles, we examined recombination in *spo11-HA/spo11-HA* (hereafter, *spo11-HA*) and heterozygous *spo11-Y135F-HA/spo11-HA* (hereafter, *spo11-yf*) mutant strains. In tetrads from a *spo11-yf* strain, where DSBs globally are reduced to ~30% of wild-type levels (Martini *et al.* 2006), the fraction of Gfp*$^+$ spores with a crossover configuration was 66.7%, significantly higher than in *SPO11*$^+$ (Table 2A). Thus, P^{GPD1}*-gfp** heteroalleles can display the altered recombination outcomes diagnostic of crossover homeostasis. Interestingly, however, the crossover fraction was not increased in the *spo11-HA* strain (in which global DSBs are ~80% of wild type), unlike with the *arg4* heteroalleles (compare Table 2, A and B). Possible reasons for this difference are addressed in the *Discussion*.

Crossover homeostasis can also be assessed by comparing genetic distances in wild type and *spo11* hypomorphs (Martini *et al.* 2006). In unselected tetrads (*i.e.*, irrespective of whether a Gfp*$^+$ recombinant had formed), no significant difference was observed between *SPO11*$^+$ and *spo11-HA* strains in the *CEN8*::*RFP*–*THR1*::*CFP* interval (Figure 5H). This result is consistent with the occurrence of crossover homeostasis.

Evaluating incidental exchanges: When recombination generates a functional *GFP** allele, the linkage of the flanking markers on the *GFP**-bearing chromatid can be altered by a second recombination event (specifically, a crossover) within the *RFP–CFP* interval. Such incidental exchanges can

Table 2 Heteroallele recombination assays for crossovers and noncrossovers

A. *gfp** heteroalleles

MSH5 genotype	*SPO11* genotype	No. of noncrossovers (%)		No. of crossovers (%)		Total	% Crossover (observed)	% Crossover (corrected)	Significance	MI nondisjunction	Double Gfp*+
		Rfp+ Cfp−	Rfp− Cfp+	Rfp+ Cfp+	Rfp− Cfp−						
Wild type	Wild type	301 (29.7)	89 (8.8)	41 (4.0)	582 (57.4)	1013	61.5 (623/1013)	59.1–59.2		0/684	19/684 (2.8%)
	spo11-HA	360 (35.1)	63 (6.1)	29 (2.8)	574 (55.9)	1026	58.8 (603/1026)	56.8–57.1	$P = 0.2$	0/752	11/752 (1.5%)
	spo11-yf	286 (27.6)	58 (5.6)	29 (2.8)	661 (63.9)	1034	66.7 (690/1034)	67.7–68.2	$P = 0.01$	6/1060 (0.6%)	20/1060 (1.9%)
*msh5*Δ	Wild type	496 (46.7)	124 (11.7)	25 (2.4)	418 (39.3)	1063	41.7 (443/1063)	40.0	$P = 0.0001$	75/1178 (6.4%)	40/1178 (3.4%)

B. *arg4* heteroalleles

MSH5 genotype	*SPO11* genotype	No. of noncrossovers (%)		No. of crossovers (%)		Total	% Crossover (observed)	% Crossover (corrected)	Significance
		Ura+ Thr+	Ura− Thr−	Ura− Thr+	Ura+ Thr−				
Wild type	Wild type	179 (3.0)	2690 (44.6)	2862 (47.4)	306 (5.1)	6037	52.5 (3168/6037)	46.2 (2790/6037)	
	spo11-HA	270 (4.3)	2432 (39.1)	3242 (52.1)	276 (4.4)	6220	56.6 (3518/6220)	50.0 (3111/6220)	$P = 0.0001$
	spo11-yf	165 (3.5)	1697 (36.1)	2613 (55.6)	227 (4.8)	4702	60.4 (2840/4702)	53.4 (2511/4702)	$P = 0.0001$
*msh5*Δ	Wild type	148 (11.0)	675 (50.3)	479 (35.7)	39 (2.9)	1341	38.6 (518/1341)	34.2 (458/1341)	$P = 0.0001$

(A) Gfp*+ tetrads from strains carrying the recombination reporter diagrammed in Figure 5A were enriched by FACS, and then the configuration of flanking markers was scored by microscopy. Crossover/noncrossover data were pooled from two independent cultures of each strain (≥281 tetrads per culture). For MI nondisjunction and double Gfp*+ counts, only a subset of tetrads was scored. MI nondisjunction and double Gfp*+ events were omitted from totals for calculating crossover percentages. Crossover percentages were corrected for incidental exchanges as described in the *Appendix*. Statistical significance was evaluated by Fisher's exact test (two-tailed *P*-value) for the proportion of crossovers (observed) for each strain compared to wild type.

(B) Random spores from strains carrying the recombination reporter diagrammed in Figure S1 were scored as previously described by Martini *et al.* (2006). Data were pooled from three or more independent cultures of each strain (≥193 spore clones/culture). Correction for incidental exchanges was calculated using previously published correction factors (10% of the Ura−Thr1+ clones and 30% of the Ura+Thr1− clones were scored as noncrossovers) (Martini *et al.* 2006). Statistical significance was evaluated by chi square with Yates' correction for the proportion of crossovers (observed) for each strain compared to wild type. It should be noted that the crossover percentages reported for *SPO11*, *spo11-HA*, and *spo11-yf* are slightly lower than those previously reported by Martini *et al.* (2006). Fisher's exact test (two tailed *P*-value), $P < 0.04$. Reasons for this difference are not known.

Table 3 Analysis of incidental crossovers

Gfp*+ spore class	*Nde*I digest (site1/site2)	No. of spore clones (% of class)		Configuration of markers is consistent with:
		SPO11+	*spo11-HA*	
Rfp− Cfp−	Cut/cut	67/72 (93.0)	53/53 (100.0)	Single crossover associated with *GFP** conversion
	Cut/uncut	2/72 (2.8)	0/53	Noncrossover conversion of *gfp*-atg* with distal incidental exchange
	Uncut/cut	3/72 (4.2)	0/53	Noncrossover conversion of *gfp*-R215X* with proximal incidental exchange
Rfp+ Cfp+	Uncut/uncut	2/2 (100.0)	8/9 (88.9)	Single crossover associated with *GFP** conversion
	Cut/uncut	0/2	1/9 (11.1)	Noncrossover conversion of *gfp*-atg* with proximal incidental exchange
Rfp+ Cfp−	Uncut/cut	43/46 (93.5)	42/45 (93.3)	Noncrossover conversion of *gfp*-R215X*
	Cut/cut	3/46 (6.5)	3/45 (6.7)	Crossover associated with *GFP** conversion with proximal incidental exchange
Rfp− Cfp+	Cut/uncut	9/9 (100.0)	20/23 (87.0)	Noncrossover conversion of *gfp*-atg*
	Cut/cut	0/9	2/23 (8.7)	Crossover associated with *GFP** conversion with distal incidental exchange
	Uncut/uncut	0/9	1/23 (4.3)	Crossover associated with *GFP** conversion with proximal incidental exchange

Single Gfp*+ spores of the four possible flanking marker configurations were sorted, allowed to grow, and then genotyped for the *Nde*I sites diagrammed in Figure 5A. Data were pooled from two independent cultures (≥39 spores analyzed per culture). The agreement with expected marker patterns is described for each class.

cause a noncrossover Gfp*+ conversion to appear to be a crossover or, conversely, "erase" a crossover at *gfp**. Incidental exchanges thus complicate estimates of what fraction of recombination events yield a crossover.

This issue could be addressed with the *arg4* heteroalleles because of inclusion of nearby *Nde*I restriction site polymorphisms (Figure S1) (Martini *et al.* 2006). A crossover associated with an Arg+ conversion usually exchanges the *Nde*I polymorphisms along with the more distant markers, whereas incidental exchange outside the region between the *Nde*I sites would leave a parental *Nde*I configuration (for more detail, see figure S1 of Martini *et al.* 2006). We created *gfp** heteroalleles flanked by the same *Nde*I site polymorphisms (Figure 5A) and determined the configuration of markers in flow-sorted Gfp*+ single-spore clones (Table 3). For the most common crossover configuration (Rfp− Cfp−), 7.0% had a parental configuration of the *Nde*I sites, consistent with noncrossover conversion of *gfp** plus an incidental exchange. Similarly, 6.5% of spores with the most common noncrossover configuration (Rfp+ Cfp−) had the pattern expected for a crossover *gfp** conversion that was erased by a second, incidental exchange (Table 3). *SPO11+* and *spo11-HA* strains did not differ significantly (Table 3), consistent with prior findings with *arg4* heteroalleles (Martini *et al.* 2006).

Determining the configuration of *Nde*I markers is laborious and time-consuming, making it difficult to compile large data sets and thus reducing statistical power. The fluorescence-based assay circumvents this limitation by allowing estimation of incidental exchange from the segregation patterns in Gfp*+ tetrads (*Appendix*). By this analysis, 6.9% of observed crossovers and 4.7% of observed noncrossovers appear to be due to incidental exchange in wild type, similar to results from the restriction site assay. Importantly, none of the mutants analyzed in this study were significantly different from wild type in this regard (*Appendix*).

Resolving segregation classes that are ambiguous in random spore analysis: An advantage of the *gfp** heteroallele assay is that it allows identification of premeiotic and complex meiotic recombination events, which appear as tetrads containing two Gfp*+ spores (Figure 5F). Such events would be indistinguishable from simple conversions in a random spore analysis. The frequency of double Gfp*+ tetrads was similar in all of the strains analyzed (Table 2A, $P > 0.1$). These tetrads were excluded from further analyses.

Chromosome missegregation can inject ambiguity into a random spore analysis by yielding spore genotypes indistinguishable from certain recombinant configurations. For example, in the *arg4* heteroallele assay, Ura+ Arg+ Thr+ spore clones can arise via noncrossover conversion at *arg4*, or by an Arg+ conversion along with chromosome VIII MI nondisjunction (Figure S1). Effects of this ambiguity are demonstrated in Table 2B: the high frequency of MI nondisjunction in the *msh5Δ* strain causes it to show a much greater increase relative to wild type in the Ura+ Thr+ noncrossover class (3.7-fold) than in the Ura− Thr− noncrossover class (1.1-fold). Additional tests (*e.g.*, directly measuring ploidy) are required to resolve this ambiguity and to accurately measure crossover:noncrossover ratios.

The fluorescence-based recombination assay circumvents this issue because segregation of all four chromatids can be followed, allowing ready detection of MI nondisjunction (Figure 5G). MI nondisjunction was not observed in the *SPO11* and *spo11-HA* strains (<0.15%), but occurred at a low frequency in the *spo11-yf* strain (Table 2A) as expected from its reduced spore viability (Diaz *et al.* 2002). MI nondisjunction was elevated in a *msh5Δ* mutant as expected, but the frequency was lower than with the missegregation-specific assay described above (compare Table 2A and Figure 2B). The reason for the discrepancy is that we selected tetrads with a detectable recombination event at *gfp**, many of which successfully experienced a crossover that can promote proper segregation of chromosome VIII. If we disregard the crossover tetrads (443/1138) and assume that the remainder have a nondisjunction probability of 0.108 (see Figure 2B), then we expect to recover 75 MI nondisjunction events, precisely as observed (Table 2A). Reasoning in the opposite direction, the MI nondisjunction frequency that would have been observed in unselected

tetrads can be estimated as $NDJ_{obs}/(total - CO_{obs})$, where NDJ_{obs} is the observed number of nondisjunction tetrads and CO_{obs} is the number of tetrads with a crossover configuration for the Gfp*$^{+}$ spore.

Discussion

Here we have shown that recombination and chromosome missegregation can be scored in tetrads largely independently of spore viability by using a set of spore-autonomous fluorescent constructs. For these analyses, the rate-limiting step is moving mutations of interest into the fluorescent tester strains. Once strain construction is completed, a comprehensive analysis can be performed in ~2 hr following sporulation (500 events counted per hour). The system is potentially amenable to automated scoring, which would further increase throughput. Removing tetrad dissection and subsequent scoring as rate-limiting steps opens the door to rapidly interrogating strains under a wide variety of environmental conditions, which is of interest given that temperature and other factors are known to affect meiotic chromosome dynamics in wild-type and certain mutants (Abdullah and Borts 2001; Börner *et al.* 2004; Chan *et al.* 2009; Cotton *et al.* 2009).

The fluorescent constructs that we developed are modular and portable, allowing one to rapidly tailor the assays described here to different genomic regions. Another advantage of using spore-autonomous cassettes is that the addition of a third fluorescent marker allows for chromosome missegregation and crossover frequency to be scored simultaneously. A different method to follow meiotic chromosome segregation involves visualizing the binding of LacI-GFP to an array of *lac* operator (*lacO*) sequences integrated near the centromere of a particular chromosome (Straight *et al.* 1996). This system permits rapid analysis of MI nondisjunction and PSSC and MII nondisjunction and, unlike spore-autonomous fluorescent protein expression, the segregation of marked chromosomes can be followed in real time. However, our system has complementary advantages over the LacI/*lacO* system. For example, tandem repeats can influence the position of nucleosomes and transcriptional activity (Vinces *et al.* 2009), so there is potential for these large repeat arrays to perturb chromosome dynamics, although to our knowledge this issue has not been rigorously tested. In contrast, our fluorescent constructs are smaller and lack repetitive elements, making this method potentially less invasive. Moreover, adding more markers would likely be difficult to achieve with operator arrays, although it is feasible, in principle, given a suitable collection of different operators and fusions of fluorescent proteins to sequence-specific DNA-binding modules.

*Recombinants at arg4 and gfp**

Several asymmetries were observed in the recombinant tetrad populations. For example, noncrossover Gfp*$^{+}$ spores were strongly biased such that 77% had an Rfp^{+} Cfp^{-} configuration (Table 2A). This is the expected pattern, given the distribution of DSBs relative to the heteroallele sequence polymorphisms and given that the broken chromosome is the recipient of genetic information in a gene conversion event. As noted above, *gfp*-R215X* is the mutation closest to the nearest DSB site (Figure 5, A and B), so conversion of this mutation to wild type accounts for a majority of the noncrossover Gfp*$^{+}$ recombinants, which inherit the parental configuration from the original *gfp*-R215X* chromosome (*i.e.*, Rfp^{+} Cfp^{-}). DSBs to the right of P^{GPD1}-*gfp** are much farther from the *gfp*-atg* mutation (Figure 5, A and B) and therefore contribute a smaller number of noncrossovers in which the *gfp*-atg* mutation is converted to wild type, yielding the Rfp^{-} Cfp^{+} configuration.

Bias was even stronger for crossover Gfp*$^{+}$ spores, with 93% negative for both RFP and CFP (Table 2A). This pattern is also as expected from the distribution of DSBs. Crossover Gfp*$^{+}$ recombinants that arise from gene conversion of the *gfp*-R215X* mutation usually have the crossover breakpoint to the left of the *gfp*-atg* mutation, which leaves the functional *GFP** allele on a chromatid that lacks both flanking markers (Figure 5A). Similarly, crossover Gfp*$^{+}$ recombinants that arise from gene conversion of the *gfp*-atg* allele usually have the crossover breakpoint to the right of the *gfp*-R215X* mutation, which again leaves the functional *GFP** allele flanked by neither *RFP* nor *CFP*. Finally, functional *GFP** can also be generated by crossing over between the two mutations without gene conversion, which would also leave *GFP** flanked by neither *RFP* nor *CFP*. The stronger bias among crossovers than noncrossovers is explained by the fact that multiple ways to achieve crossover-associated generation of *GFP** all favor the same configuration of flanking markers, whereas noncrossover *GFP** products have opposite configurations, depending on which allele is converted.

Comparing the *gfp** and *arg4* assays, we observed a greater fraction of Gfp*$^{+}$ recombinants with a crossover configuration than was seen for Arg^{+} recombinants (Table 2, A and B). A possible reason for this difference is discussed below. As previously noted (Martini *et al.* 2006), *arg4* heteroalleles also show biased recovery of particular recombinant configurations (Table 2B). The specific patterns are different for *arg4 vs. gfp** [*e.g.*, *arg4* heteroalleles showed stronger bias in the noncrossover class (94%) and slightly less bias in the crossover class (90%)], in keeping with the different spatial relationship of DSBs to sequence polymorphisms for the two recombination reporter systems.

Crossover homeostasis and crossover:noncrossover ratios at individual loci

A previous study found that the endogenous *ARG4* locus exhibits crossover homeostasis, but the artificial hotspot *HIS4LEU2* does not (Martini *et al.* 2006). We show here that, when DSBs are reduced by *spo11* mutation, a different artificial hotspot shows an increased crossover:noncrossover ratio diagnostic of crossover homeostasis. It is possible that

HIS4LEU2 does not respond normally to crossover control mechanisms, but an alternative possibility is that DSBs at this site are subject to the same control mechanisms, but are more likely to influence other recombination events nearby than to be influenced by them (Martini *et al.* 2006). In any case, our results demonstrate that the spore-autonomous fluorescence cassettes are amenable to detecting and quantifying crossover homeostasis.

Interestingly, however, the *gfp** heteroalleles did not show altered crossover:noncrossover ratios in the *spo11-HA* background. Why is *gfp** different from *arg4* in this respect? One possibility is that the fluorescent protein expression cassettes alter the ability of the *CEN8-THR1* genomic interval to experience decreased DSB formation in response to this *spo11* mutation. Although the *spo11-HA* allele appears to reduce DSBs to a roughly similar degree in many locations, locus-specific differences have been documented (Martini *et al.* 2006).

Another possibility lies in the different ways that the *gfp** and *arg4* heteroallele systems are affected by gene conversion tract lengths. The majority of Arg^+ conversions are generated from DSBs within the *arg4* promoter, averaging ~185 bp from the mutation that is most frequently converted (Nicolas *et al.* 1989; Martini *et al.* 2006; Pan *et al.* 2011). Most conversion tracts must thus extend at least 185 bp and no more than ~1465 bp (to prevent co-conversion of the second mutation, which would result in an Arg^- recombinant). In contrast, most Gfp^{*+} conversions are generated either from a DSB site ~50–200 bp to the left of the *gfp*-R215X* mutation or, less frequently, from a DSB site located ~900–1100 bp to the right of the *gfp*-atg* mutation. The two *gfp** mutations are 641 bp apart. Most detectable conversions thus have tract lengths between 50 and 841 bp or between 900 and 1741 bp. Both single-locus and whole-genome studies have shown that the median conversion tract length is longer for crossovers (~2.0 kb) than for noncrossovers (~1.8 kb) (Borts and Haber 1989; Chen *et al.* 2008; Mancera *et al.* 2008). The lengths of individual conversion tracts vary over a wide range, however. The *gfp** heteroalleles detect a narrower subset of possible conversion events than the *arg4* heteroalleles, which may account for why these reporters yield different fractions of crossover-associated recombinants in wild type (Table 2, A and B). In principle, then, these recombination reporters may respond differently if the distribution of conversion tract lengths changes in a mutant and, in particular, if crossover and noncrossover tract lengths are differentially affected. Determining whether this scenario can account for the different effect of the *spo11-HA* mutation on crossing over at *arg4 vs. gfp** will require testing whether distributions of conversion tract lengths are altered in *spo11-HA* strains. One approach to reduce the impact of conversion tract length (and thus the frequency of co-conversions) is to measure non-Mendelian segregation (1:3 or 3:1, *i.e.*, gene conversion) in strains heterozygous for a wild-type fluorescent protein allele and an allele with a single point mutation.

Future applications

A fluorescence-enabled dissection scope would make it possible to isolate and grow spores with interesting recombination events. There is also ample precedent that genomic regions can differ from one another in basic recombination patterns and in responses to perturbations or to mutations in *trans*-acting factors (Borts and Haber 1989; Martini *et al.* 2006; Chen *et al.* 2008; Mancera *et al.* 2008; Zanders and Alani 2009). Although only a single chromosome and set of loci are described here for each assay, the adaptability and portability of the spore-autonomous expression cassettes opens up essentially any portion of the genome to interrogation. Finally, we note that, with application of high-throughput fluorescence imaging techniques, these constructs could also be used as a quantitative phenotypic output for forward genetic screens.

Acknowledgments

We are grateful to Sean Burgess, Owen Hughes, and Kelly Komachi for sharing information and constructs for spore-autonomous expression prior to publication. We thank Jan Hendrikx and Jennifer Wilshire of the Memorial Sloan-Kettering Cancer Center Flow Cytometry Core for technical assistance. This work was supported by National Institutes of Health grant R01 GM058673. S.K. is an Investigator of the Howard Hughes Medical Institute.

Literature Cited

Abdullah, M. F., and R. H. Borts, 2001 Meiotic recombination frequencies are affected by nutritional states in *Saccharomyces cerevisiae*. Proc. Natl. Acad. Sci. USA 98: 14524–14529.

Berchowitz, L. E., and G. P. Copenhaver, 2008 Fluorescent Arabidopsis tetrads: a visual assay for quickly developing large crossover and crossover interference data sets. Nat. Protoc. 3: 41–50.

Borde, V., T. C. Wu, and M. Lichten, 1999 Use of a recombination reporter insert to define meiotic recombination domains on chromosome III of *Saccharomyces cerevisiae*. Mol. Cell. Biol. 19: 4832–4842.

Börner, G. V., N. Kleckner, and N. Hunter, 2004 Crossover/noncrossover differentiation, synaptonemal complex formation, and regulatory surveillance at the leptotene/zygotene transition of meiosis. Cell 117: 29–45.

Borts, R. H., and J. E. Haber, 1989 Length and distribution of meiotic gene conversion tracts and crossovers in *Saccharomyces cerevisiae*. Genetics 123: 69–80.

Chan, A. C., R. H. Borts, and E. Hoffmann, 2009 Temperature-dependent modulation of chromosome segregation in *msh4* mutants of budding yeast. PLoS ONE 4: e7284.

Chen, S. Y., T. Tsubouchi, B. Rockmill, J. S. Sandler, D. R. Richards *et al.*, 2008 Global analysis of the meiotic crossover landscape. Dev. Cell 15: 401–415.

Cotton, V. E., E. R. Hoffmann, M. F. Abdullah, and R. H. Borts, 2009 Interaction of genetic and environmental factors in *Saccharomyces cerevisiae* meiosis: the devil is in the details. Methods Mol. Biol. 557: 3–20.

Diaz, R. L., A. D. Alcid, J. M. Berger, and S. Keeney, 2002 Identification of residues in yeast Spo11p critical for meiotic DNA double-strand break formation. Mol. Cell. Biol. 22: 1106–1115.

Francis, K. E., S. Y. Lam, B. D. Harrison, A. L. Bey, L. E. Berchowitz *et al.*, 2007 Pollen tetrad-based visual assay for meiotic recombination in Arabidopsis. Proc. Natl. Acad. Sci. USA 104: 3913–3918.

Gordon, O., C. Taxis, P. J. Keller, A. Benjak, E. H. Stelzer *et al.*, 2006 Nud1p, the yeast homolog of Centriolin, regulates spindle pole body inheritance in meiosis. EMBO J. 25: 3856–3868.

Griesbeck, O., G. S. Baird, R. E. Campbell, D. A. Zacharias, and R. Y. Tsien, 2001 Reducing the environmental sensitivity of yellow fluorescent protein. Mechanism and applications. J. Biol. Chem. 276: 29188–29194.

Hawley, R. S., 2007 Meiosis in living color: fluorescence-based tetrad analysis in Arabidopsis. Proc. Natl. Acad. Sci. USA 104: 3673–3674.

Hollingsworth, N. M., L. Ponte, and C. Halsey, 1995 MSH5, a novel MutS homolog, facilitates meiotic reciprocal recombination between homologs in *Saccharomyces cerevisiae* but not mismatch repair. Genes Dev. 9: 1728–1739.

Jones, G. H., 1984 The control of chiasma distribution. Symp. Soc. Exp. Biol. 38: 293–320.

Keeney, S., C. N. Giroux, and N. Kleckner, 1997 Meiosis-specific DNA double-strand breaks are catalyzed by Spo11, a member of a widely conserved protein family. Cell 88: 375–384.

Lynn, R. R., and P. T. Magee, 1970 Development of the spore wall during ascospore formation in *Saccharomyces cerevisiae*. J. Cell Biol. 44: 688–692.

Malkova, A., J. Swanson, M. German, J. H. McCusker, E. A. Housworth *et al.*, 2004 Gene conversion and crossing over along the 405-kb left arm of *Saccharomyces cerevisiae* chromosome VII. Genetics 168: 49–63.

Mancera, E., R. Bourgon, A. Brozzi, W. Huber, and L. M. Steinmetz, 2008 High-resolution mapping of meiotic crossovers and noncrossovers in yeast. Nature 454: 479–485.

Marston, A. L., and A. Amon, 2004 Meiosis: cell-cycle controls shuffle and deal. Nat. Rev. Mol. Cell Biol. 5: 983–997.

Martini, E., R. L. Diaz, N. Hunter, and S. Keeney, 2006 Crossover homeostasis in yeast meiosis. Cell 126: 285–295.

Mell, J. C., K. Komachi, O. Hughes, and S. Burgess, 2008 Cooperative interactions between pairs of homologous chromatids during meiosis in *Saccharomyces cerevisiae*. Genetics 179: 1125–1127.

Moens, P. B., 1971 Fine structure of ascospore development in the yeast *Saccharomyces cerevisiae*. Can. J. Microbiol. 17: 507–510.

Murakami, H., V. Borde, A. Nicolas, and S. Keeney, 2009 Gel electrophoresis assays for analyzing DNA double-strand breaks in *Saccharomyces cerevisiae* at various spatial resolutions. Methods Mol. Biol. 557: 117–142.

Neiman, A. M., 2005 Ascospore formation in the yeast *Saccharomyces cerevisiae*. Microbiol. Mol. Biol. Rev. 69: 565–584.

Nicolas, A., D. Treco, N. P. Schultes, and J. W. Szostak, 1989 An initiation site for meiotic gene conversion in the yeast *Saccharomyces cerevisiae*. Nature 338: 35–39.

Nishant, K. T., C. Chen, M. Shinohara, A. Shinohara, and E. Alani, 2010 Genetic analysis of baker's yeast Msh4-Msh5 reveals a threshold crossover level for meiotic viability. PLoS Genet. 6: pii: e1001083.

Page, S. L., and R. S. Hawley, 2003 Chromosome choreography: the meiotic ballet. Science 301: 785–789.

Pan, J., M. Sasaki, R. Kniewel, H. Murakami, H. G. Blitzblau *et al.*, 2011 A hierarchical combination of factors shapes the genome-wide topography of yeast meiotic recombination initiation. Cell 144: 719–731.

Roig, I., and S. Keeney, 2008 Probing meiotic recombination decisions. Dev. Cell 15: 331–332.

Schneider, J. C., and L. Guarente, 1991 Vectors for expression of cloned genes in yeast: regulation, overproduction, and underproduction. Methods Enzymol. 194: 373–388.

Sikorski, R. S., and P. Hieter, 1989 A system of shuttle vectors and yeast host strains designed for efficient manipulation of DNA in *Saccharomyces cerevisiae*. Genetics 122: 19–27.

Snowden, T., S. Acharya, C. Butz, M. Berardini, and R. Fishel, 2004 hMSH4-hMSH5 recognizes Holliday Junctions and forms a meiosis-specific sliding clamp that embraces homologous chromosomes. Mol. Cell 15: 437–451.

Straight, A. F., A. S. Belmont, C. C. Robinett, and A. W. Murray, 1996 GFP tagging of budding yeast chromosomes reveals that protein-protein interactions can mediate sister chromatid cohesion. Curr. Biol. 6: 1599–1608.

Sym, M., and G. S. Roeder, 1994 Crossover interference is abolished in the absence of a synaptonemal complex protein. Cell 79: 283–292.

Vinces, M. D., M. Legendre, M. Caldara, M. Hagihara, and K. J. Verstrepen, 2009 Unstable tandem repeats in promoters confer transcriptional evolvability. Science 324: 1213–1216.

Wach, A., A. Brachat, R. Pohlmann, and P. Philippsen, 1994 New heterologous modules for classical or PCR-based gene disruptions in *Saccharomyces cerevisiae*. Yeast 10: 1793–1808.

Wu, T. C., and M. Lichten, 1995 Factors that affect the location and frequency of meiosis-induced double-strand breaks in *Saccharomyces cerevisiae*. Genetics 140: 55–66.

Zanders, S., and E. Alani, 2009 The *pch2Δ* mutation in baker's yeast alters meiotic crossover levels and confers a defect in crossover interference. PLoS Genet. 5: e1000571.

Communicating editor: G. P. Copenhaver

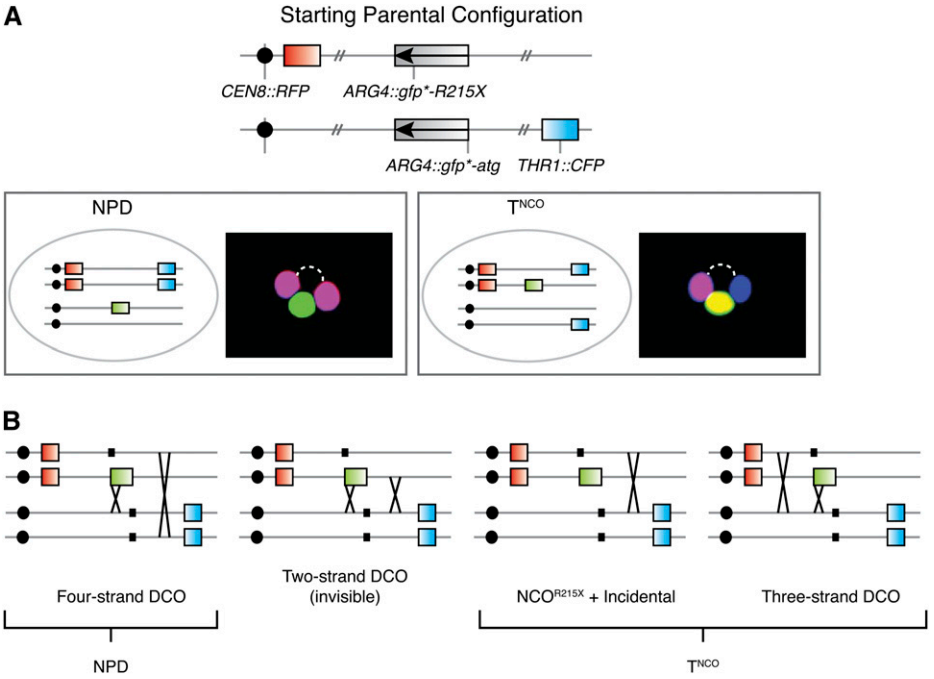

Figure A1 Classification of Gfp*$^{+}$ tetrads with at least two detectable recombination events. (A) Schematic of parental marker configuration and schematic representations and micrographs illustrating the configuration of markers when a recombination event at *gfp** is associated with a second recombination event in the *CEN8–THR1* interval. The two informative classes of tetrads (NPD and T^{NCO}) are shown. (B) NPDs arise from two crossovers between *CEN8* and *THR1* involving all four chromatids [four-strand double crossovers (DCO)]. T^{NCO} tetrads arise from noncrossover (NCO) gene conversion (either NCO^{R215X} or NCO^{atg}) plus an incidental crossover or from a subset of three-strand DCOs (see Figure A2). Tetrads that have a crossover Gfp*$^{+}$ recombinant plus an incidental crossover involving the same pair of chromatids (two-strand DCO) are indistinguishable from NCO gene conversion; *i.e.*, they have "invisible" crossovers. Small black boxes represent positions of the *gfp*-R215X* and *gfp*-atg* mutations.

Appendix: Estimating Frequencies of Incidental Exchanges from Gfp*$^{+}$ Tetrad Data

Because we can assess all four spores, we can evaluate the occurrence of Gfp*$^{+}$ recombinants that are incorrectly scored because of incidental exchanges. Two classes of tetrad are informative for this purpose: those with a NPD configuration of *RFP* and *CFP* and those that are tetratype for *RFP* and *CFP* but have a noncrossover configuration of the Gfp*$^{+}$ chromatid (T^{NCO}) (Figure A1A). NPD tetrads arise from two crossovers involving all four chromatids (four-strand double crossover; Figure A1B). T^{NCO} tetrads can arise from a noncrossover *gfp** conversion plus a separate crossover involving the *GFP**-bearing chromatid's sister or from a subset of cells that experienced two crossovers involving three chromatids (three-strand double crossovers) (Figure A1B).

The NPD and T^{NCO} tetrad classes are indicative of meioses where at least two separate recombination events occurred within the genetic interval of interest. Thus, examining the frequencies of these tetrad classes provides a simple test to determine whether it is likely that different strains or different experiments display variability in the frequency of incidental exchanges. By this criterion, neither the *spo11* hypomorphs nor the *msh5Δ* strain was significantly different from wild type (Table A1). This result suggests that we need not worry that our ability to evaluate changes in crossover:noncrossover ratios is compromised by variable frequencies of incidental exchange.

Nevertheless, the data allow us to quantitatively estimate the contribution of incidental exchanges. In the discussion that follows, we will consider only situations with a maximum of two recombination events in the *RFP–CFP* interval per tetrad (either two crossovers or one noncrossover at *gfp** plus a crossover somewhere else). Our goal is to estimate the frequency of true crossover-associated Gfp*$^{+}$ recombinants (CO_{true}). To do so, we must correct the observed frequency of crossovers (CO_{obs}) by adding back tetrads in which a crossover at *GFP** was erased by incidental exchange and by removing tetrads in which an incidental exchange falsely caused a *GFP** noncrossover to appear to be a crossover:

$$CO_{true} = CO_{obs} + [\text{erased crossovers}] - [\text{false crossovers}] \quad \text{(A1)}.$$

Table A1 Frequency of tetrads with at least two detectable recombination events

MSH5 genotype	*SPO11* genotype	No. of NPD (%)	No. of T^{NCO}(%)
Wild type	Wild type	4/462 (0.9)	24/462 (5.2)
	spo11-HA	9/745 (1.2), $P = 0.78$	44/745 (5.9), $P = 0.70$
	spo11-yf	16/743 (2.2), $P = 0.11$	44/743 (5.9), $P = 0.70$
msh5Δ	Wild type	6/766 (0.8), $P = 1.00$	31/766 (4.0), $P = 0.39$

Gfp*$^{+}$ tetrads were enriched by FACS from one culture for wild type, *spo11-HA*, and *spo11-yf* and from two independent cultures for *msh5Δ* (≥302 tetrads analyzed per culture). Statistical significance was evaluated by a Fisher's exact test (two-tailed *P*-value) that compared each strain to wild type. Note that the observed NPDs may underrepresent total NPDs because a small fraction of tetrads that appear to display MI nondisjunction (Figure 5G) could have arisen from a four-strand double crossover instead. Such NPD tetrads are expected to be exceedingly rare, however, because they contain a Gfp*$^{+}$ spore that is also Rfp^{+} Cfp^{+}, which is an uncommon configuration (≥14-fold less common than the Rfp^{-} Cfp^{-}configuration; see Table 2A). All such tetrads were thus scored as "MI nondisjunction."

There are two configurations by which an incidental exchange can erase a crossover at *GFP**. First, the incidental exchange can involve the same two chromatids as at *GFP** (a two-strand double crossover; Figure A1B). Such events are indistinguishable from tetrads in which only a noncrossover conversion has occurred. Second, the incidental exchange can include one of the chromatids involved in the *GFP** crossover, plus a different chromatid (three-strand double crossover). All three-strand double crossovers yield a tetratype configuration of *RFP* and *CFP*, but only a subset show a false noncrossover arrangement of the Gfp^{*+} chromatid, depending on which *gfp** allele is converted, which chromatids cross over, and whether the second crossover occurs to the left or the right of the crossover at *GFP** (see Figure A2A).

Thus, the number of erased crossovers can be estimated as the number of two-strand double crossovers plus the fraction of three-strand double crossovers that did in fact erase the crossover at *GFP** [we use k ($0 \leq k \leq 1$) to denote this fraction]. If we assume that there is no chromatid interference (Chen *et al.* 2008), then two-strand double crossovers occur at the same frequency as four-strand double crossovers, *i.e.*, NPDs. Moreover, the frequency of all three-strand double crossovers should be twice the frequency of four-strand double crossovers. Thus:

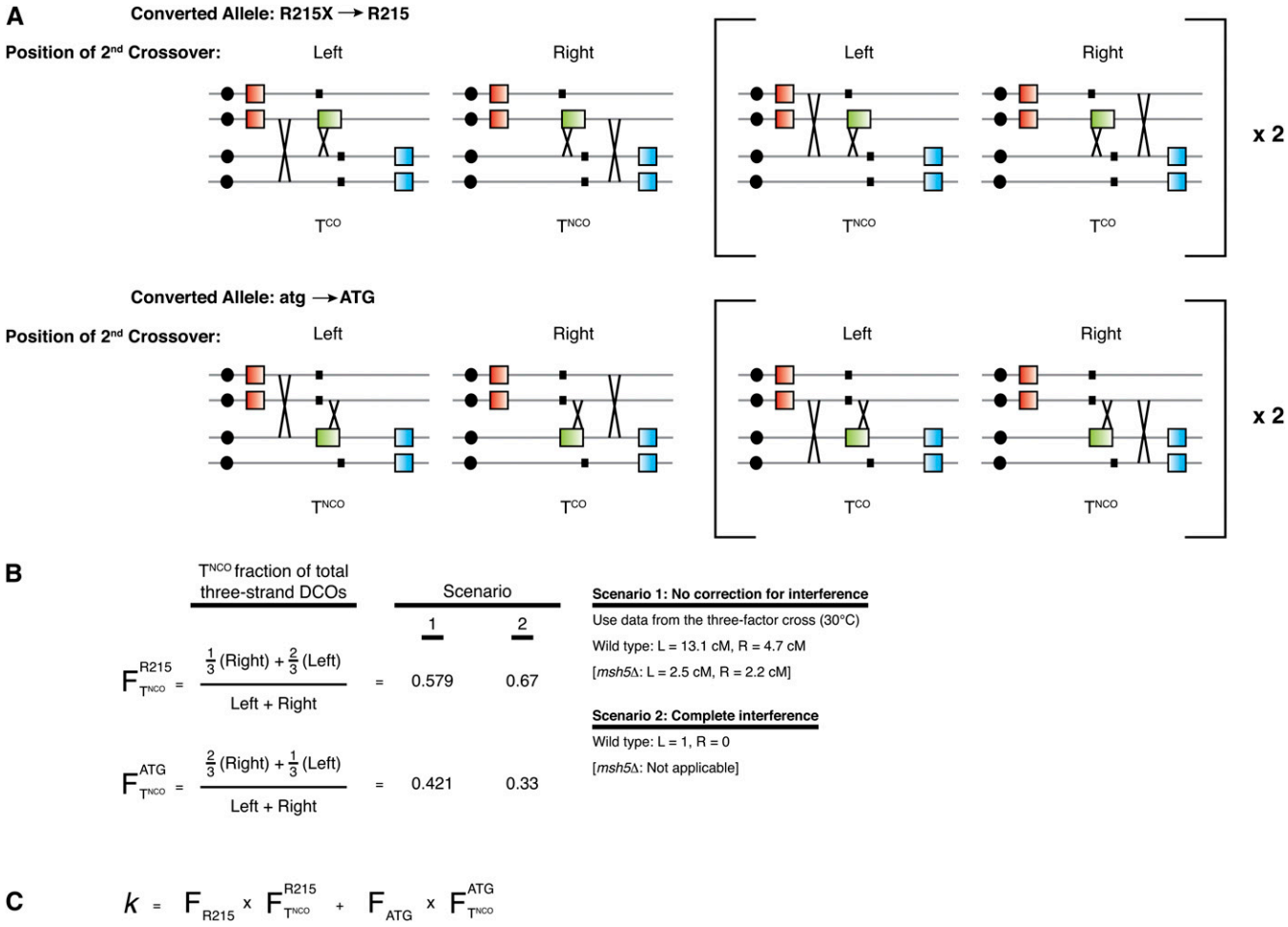

Figure A2 Estimating the fraction (k) of three-strand DCOs that erase a crossover at *GFP**. (A) Schematic representations of three-strand DCOs, all of which give rise to a tetratype (T) configuration of *RFP* and *CFP*. A subset has the same configuration as noncrossover *GFP** conversion plus an incidental exchange (T^{NCO}), and the remainder look like tetrads with just a single crossover (T^{CO}). Which configuration arises depends on three factors: which *gfp** allele is converted to *GFP**, whether the incidental exchange occurs to the right or the left of the crossover at *GFP**, and which chromatids are involved in the two crossovers. Each situation is diagrammed separately. Events diagrammed inside the brackets (Right) are three-strand DCOs where the incidental exchange involves the gene-converted chromatid's sister. In the absence of chromatid interference, these events are expected to occur at twice the frequency of three-strand DCOs where the incidental exchange involves the gene-converted chromatid not bracketed. (B) The fraction ($F^{allele}_{T^{NCO}}$) of three-strand DCOs expected to have a T^{NCO} configuration is calculated for each converted allele separately. For conversion of *gfp*-R215X*, a T^{NCO} configuration is expected for one-third of the tetrads with the incidental exchange located to the right side and for two-thirds of the tetrads that have incidental exchange located to the left. Thus, $F^{R215}_{T^{NCO}}$ = [1/3·(right exchange) + 2/3·(left exchange)] ÷ total. Similar logic is applied to calculate the fraction of T^{NCO} for conversion of *gfp*-atg* ($F^{ATG}_{T^{NCO}}$). To estimate the likelihood of right-side incidental exchange *vs.* left-side, we considered scenarios that ignore crossover interference or that assume strong interference (see Appendix text and B, Right). (C) k is estimated by multiplying the fraction of three-strand DCOs that appear as T^{NCO} for each allele ($F^{allele}_{T^{NCO}}$) by the fraction of all conversions that are converted for that allele (F_{allele}) and then summing the contributions for the two alleles.

Table A2 Estimates of values of *k* from tetrad data

Strain	k_1	k_2	CO_{obs}	Total	$\%CO_{obs}$	$\%CO_{corr}$
Wild type	0.543	0.591	623	1013	61.5	59.1–59.2
spo11-HA	0.555	0.617	603	1026	58.8	56.8–57.1
spo11-yf	0.552	0.610	690	1034	66.7	67.7–68.2
*msh5*Δ	0.507	NA[a]	443	1063	41.7	40.0

Values of *k* were calculated for scenario 1 (k_1) and 2 (k_2) (Figure A2B) using the formula in Figure A2C. The corrected fraction of *GFP** conversions that are crossover associated ($\%CO_{corr}$) was calculated using Equation 4.

[a] Because *msh5*Δ strains do not show crossover interference, k_2 (calculated assuming complete interference) is not applicable.

$$\text{Erased crossovers} = \text{NPD} + k \bullet 2 \bullet \text{NPD} \qquad \text{(A2)}.$$

False crossovers (noncrossover at *GFP** plus an incidental exchange involving the Gfp*$^{+}$ chromatid) are indistinguishable from tetrads with a single crossover-associated conversion, and thus their number cannot be directly measured. However, in tetrads that experienced a noncrossover at *GFP** plus an independent crossover, there is equal likelihood of the crossover involving the *GFP**-bearing chromatid or its sister. As described above, the latter event gives rise to a T^{NCO} tetrad, so the frequency of false Gfp*$^{+}$ crossovers should equal the frequency of T^{NCO} tetrads after subtracting those T^{NCO} tetrads that arise from three-strand double crossovers and that appear to be noncrossover at *GFP** (see above). Thus:

$$\text{False crossovers} = T^{NCO} - k \bullet 2 \bullet \text{NPD} \qquad \text{(A3)}.$$

Substituting into equation 1 and rearranging yields:

$$CO_{true} = CO_{obs} + (4k + 1) \bullet \text{NPD} - T^{NCO} \qquad \text{(A4)}.$$

The value of *k* depends on multiple factors, most importantly the conversion frequency for each allele and the likelihood of an incidental exchange being to the right or the left of the *GFP** conversion (Figure A2, B and C); *k* will thus differ for different recombination reporter setups. To estimate its value for our system, we assumed that the relative frequency of conversion of the *gfp*-R215X* allele *vs.* the *gfp*-atg* allele equals the relative frequency of Rfp^{+} *vs.* Cfp^{+} noncrossover spores (see *Recombinants at art4 and gfp** and Table 2A). Next, we assumed that the likelihood of the second crossover being to the left or the right of the crossover at *GFP** is proportional to the *RFP–GFP** (13.1 cM) *vs. GFP*–CFP* (4.7 cM) distances measured in the three-factor cross in Figure 4. Under these assumptions, $k = 0.543$ for the wild-type strain using the equation in Figure A2C. An alternative assumption would be that crossover interference disfavors instances where the second crossover falls in the shorter genetic interval to the right of the heteroalleles. Under this assumption, $k = 0.591$.

Table A2 shows values of *k* estimated from tetrad data from wild type, the two *spo11* hypomorphs, and *msh5*Δ. Corrected estimates of the fraction of crossover-associated Gfp*$^{+}$ recombinants are provided in Table 2A. Several conclusions emerge. First, different assumptions had little effect on the estimate of *k* and thus had little effect on the magnitude of the correction in the crossover fraction. Second, the estimates of incidental exchange frequencies from tetrad data agreed well with results from *Nde*I restriction site analysis. For example, in wild type, 6.8–6.9% of observed crossovers were estimated to be due to incidental exchange [*i.e.*, $(T^{NCO} - k{\cdot}2{\cdot}\text{NPD})/CO_{obs}$], similar to the 7.0% measured by the *Nde*I assay (Table 3). Third, this analysis suggests that incidental exchanges contribute very little quantitatively to the observed crossover *vs.* noncrossover ratio. This is in part because the total number of such events is small, but also because false crossovers and erased crossovers largely cancel one another out. As a consequence, robust conclusions about alterations of crossover:noncrossover ratios can be drawn from the uncorrected data. Nonetheless, the ease of executing the tetrad-based evaluation of incidental exchanges allows one to readily address this issue for each mutant, experimental condition, or arrangement of recombination reporters.